# Nematic-liquid-crystal light scattering in a symmetry-breaking external field

Klaus Eidner,\* M. Lewis, H. K. M. Vithana, and D. L. Johnson Department of Physics, Kent State University, Kent, Ohio 44242 (Received 3 August 1989)

A dynamic depolarized light-scattering experiment in the presence of a symmetry-breaking magnetic field was conducted on homeotropically aligned dihexylazoxybenezene (DHAOB). This experiment gives direct evidence for the presence of a lowest-order fluctuation mode and its dynamical behavior in a destabilizing magnetic field.

#### I. INTRODUCTION

It is well known that an external field applied perpendicular to the director of a nematic liquid crystal confined between two orienting surfaces must exceed a certain threshold to distort the director. The explanation of this effect is often based on the softening of some lowest-order fluctuation mode. Recently a light-scattering intensity measurement was performed which studied the fluctuation amplitudes. Earlier the relaxation of macroscopic deformations was studied. Here we present a dynamic light-scattering experiment giving direct evidence for the presence of a lowest-order fluctuation mode and its dynamical behavior in a destabilizing external magnetic field.

In Sec. II A we calculate the zero-field normal-mode spectrum of a homeotropically aligned sample of finite size in the direction of  $\hat{\mathbf{n}}_0$ , the undistorted director, under the assumption that deviations of  $\mathbf{n}$  from  $\hat{\mathbf{n}}_0$  at the boundaries require a finite amount of energy (finite anchoring) proportional to  $(\mathbf{n} \cdot \hat{\mathbf{n}}_0)^2$ . In Sec. II B we calculate the normal-mode spectrum for the case where an applied magnetic field breaks the uniaxial symmetry of the problem. The effect of finite anchoring energy and a symmetry breaking field are essential ingredients in the explanation of our light-scattering data.

In Sec. II C we discuss the differential-scattering cross section for light scattered from nematic normal modes in finite-thickness homeotropic samples. Interference effects resulting from the finite-size scattering volume are important. Section II D describes the dynamics of the nematic normal modes which are assumed to relax exponentially. This explains the digital correlation functions measured in the experiment. Section III describes the experimental geometry, gives the results of the dynamic light-scattering experiments and discusses them relative to normal-mode director dynamics and surface anchoring strength.

Section IV summarizes the conclusions drawn from the experiment and stresses the direct detection of the softening of the lowest-order normal mode by a magnetic field applied perpendicular to  $\hat{\mathbf{n}}_0$ .

### II. THEORETICAL BACKGROUND

# A. Effect of finite sample size and finite surface anchoring

We consider a nematic layer confined between the planes  $z=\pm d/2$  of a Cartesian coordinate system. Further we restrict ourselves to homeotropic alignment and small director fluctuations. Hence, the director distribution can be expressed as

$$\mathbf{n}(\mathbf{r}) = \{ \mathbf{n}_{x}(\mathbf{r}), \mathbf{n}_{y}(\mathbf{r}), 1 \}$$
 (1)

with

$$\mathbf{n}_{\mathbf{r},\mathbf{v}}(\mathbf{r}) << 1, \mathbf{n} \cdot \mathbf{n} = 1$$
.

For the description of the surface anchoring, which is assumed to be equal on both sides, we use the potential<sup>5</sup>

$$2W = -\int_{z=-d/2}^{z=+d/2} W_0 (\mathbf{n} \cdot \hat{\mathbf{n}}_0)^2 d^2 r , \qquad (2)$$

where  $\hat{\mathbf{n}}_0$  is a unit vector indicating the "easy axis" taken parallel to the z axis. The elastic free energy of the bulk is the familiar Frank free energy

$$2F_{\text{bulk}} = \int d^3r [K_{11}(\nabla \cdot \mathbf{n})^2 + K_{22}(\mathbf{n} \cdot \nabla \times \mathbf{n})^2 + K_{33}(\mathbf{n} \times \nabla \times \mathbf{n})^2].$$
(3)

The total free energy is the sum

$$F = F_{\text{bulk}} + W . \tag{4}$$

Expanding  $F_{\text{bulk}}$  to  $O(\mathbf{n}^2)$  and deviding by  $W_0$   $(k_{\alpha} \equiv K_{\alpha\alpha}/W_0)$  gives

$$\frac{2F}{W_0} = \int d^3r \{ k_1 (\partial_x n_x + \partial_y n_y)^2 + k_2 (\partial_x n_y - \partial_y n_x)^2 + k_3 [(\partial_z n_x)^2 + (\partial_z n_y)^2 \} + \int d^2r [\mathbf{n}_x^2(x, y, d/2) + n_y^2(x, y, -d/2)] . \quad (5)$$

Our goal in this section is to describe the normal-mode structure for this problem.

By symmetry the modes are uniaxial, permitting us to choose a local (in **q** space) coordinate system where  $\partial_y \rightarrow 0$  ( $q_y = 0$ ) and to treat the modes  $n_x$  and  $n_y$  separate-

ly. For a single mode of wave vector  $\mathbf{q} = (q_x, 0, q_z)$ 

$$n_x(\mathbf{r}) = g(q_z z) \exp(iq_x x) + g^*(q_z z) \exp(-iq_x x) , \qquad (6)$$

where  $g(q_z z)$  must be determined. The dependence of g on  $q_x$  is suppressed. Substituting Eq. (6) into Eq. (5) and integrating over x, we have

$$F_{x}/2L^{2} = \left[ \int_{-d/2}^{d/2} dz \left[ k_{1} q_{x}^{2} |g(q_{z}z)|^{2} + k_{3} \left| \frac{dg(q_{z}z)}{dz} \right|^{2} \right] + |g(q_{z}d/2)|^{2} + |g(-q_{z}d/2)|^{2} \right]. \tag{7}$$

 $F_y$  is given by an expression identical to Eq. (7) except that  $n_x$  is replaced by  $n_y$  and  $k_1$  by  $k_2$ .

The variational problem leading to the correct forms of  $g(q_z z)$  and the correct vaues of  $q_z$  is

$$\delta I_{x} = \delta \left[ \int_{-d/2}^{d/2} dz \left[ k_{1} q_{x}^{2} |g(q_{z}z)|^{2} + k_{3} \left| \frac{dg(q_{z}z)}{dz} \right|^{2} - \lambda |g(q_{z}z)|^{2} \right] + |g(q_{z}d/2)|^{2} + |g(-q_{z}d/2)|^{2} = 0, \quad (8)$$

where  $\lambda$  is an undetermined multiplier introduced to satisfy the constraint of Eq. (1), i.e.,  $\mathbf{n} \cdot \mathbf{n} = 1$ .

Integrating Eq. (8) by parts gives

$$\begin{split} \delta I_{x} &= \int_{-d/2}^{d/2} [(\alpha g - k_{3}g'')\delta g^{*} + (\alpha g^{*} - k_{3}g^{*}'')\delta g] dz \\ &+ [g(q_{z}d/2) + k_{3}g'(q_{z}d/2)]\delta g^{*}(q_{z}d/2) + \text{c.c.} \\ &+ [g(-q_{z}d/2) - k_{3}g'(-q_{z}d/2)]\delta g^{*}(-q_{z}d/2) \\ &+ \text{c.c.} \;, \end{split} \tag{9a}$$

where

$$\alpha \equiv k_1 q_x^2 - \lambda \ . \tag{9b}$$

Solutions of this variational problem can be found by setting the integrand in the first term to zero,

$$\alpha g - k_3 g^{\prime\prime} = 0 \tag{10}$$

and taking only solutions with definite parity relative to the z=0 symmetry plane, i.e.,  $g(q_zz)=\pm g(-q_zz)$ . The wave vector  $q_z$  must be adjusted such that the surface terms vanish to ensure the balance of the surface torque associated with the surface anchoring term against the bending torque of the director at the surface.

The solutions of Eq. (10) are  $\sin(q_z z)$  and  $\cos(q_z z)$  with  $\lambda = k_1 q_x^2 + k_3 q_z^2$ . Torque balance requires that

$$k_3 q_z = -\tan(q_z d/2) \quad (g \simeq \sin q_z z) \tag{11}$$

and

$$k_3 q_z = \cot(q_z d/2) \quad (g \simeq \cos q_z z) . \tag{12}$$

Equations (11) and (12) define a discrete set of normal-mode wave vectors  $q_z(n)$ . This set of allowed  $q_z$ 's is given by the intersection of the branches of the cotangent and negative tangent functions with a straight line of slope  $2k_3/d$  (see Fig. 1).

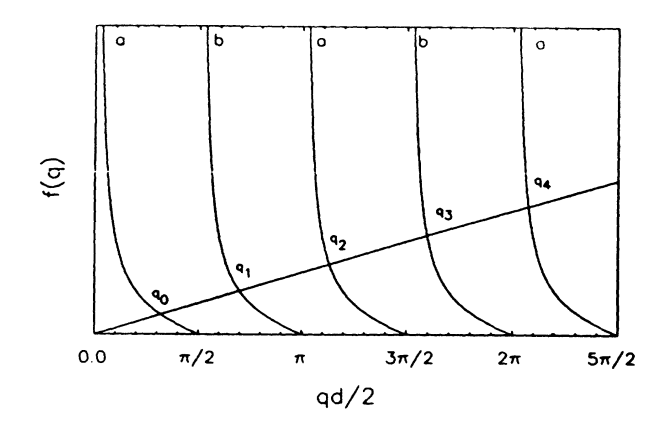


FIG. 1. Mode spectrum in a homeotropic sample with finite size in the z direction and with finite anchoring strength. Geometrical solution of Eqs. (11) and (12). Curves labeled a are cotangent [Eq. (12)] and those labeled b are negative tangents [Eq. (11)].

For infinitely strong anchoring the slope of this line is zero and the mode spectrum is given by the zeros of the tangent and cotangent functions. Hence

$$q_z(n) = (n+1)\pi/d, \quad n = 0, 1, 2, \dots,$$
 (13)

and all the fluctuation modes have zeros (nodes) at the surfaces  $z=\pm d/2$ . If the confining surfaces have no anchoring action the spectrum remains discrete with

$$q_z(n) = n\pi/d, \quad n = 0, 1, 2, \dots$$
 (14)

This occurs because now one must have zero-curvature torque at the surface, i.e.,  $g'(\pm q_z d/2)=0$ , leading to antinodes at the surfaces.

# B. Influence of a symmetry breaking external field

To continue further we must perform the usual thermodynamic calculation<sup>2</sup> for the amplitudes of each mode. Since we are restricted to small fluctuations it is unnecessary to include nonlinear terms.<sup>3</sup>

Starting from the small amplitude version of Eq. (3) and substituting one Fourier component of  $\mathbf{n}(\mathbf{r})$  the free energy is a bilinear form in  $n_x$  and  $n_y$  (Ref. 2)

$$2F_{d} = |n_{x}(\mathbf{q})|^{2} (K_{11}q_{x}^{2} + K_{22}q_{y}^{2} + K_{33}q_{z}^{2}) + |n_{y}(\mathbf{q})|^{2} (K_{11}q_{y}^{2} + K_{22}q_{x}^{2} + K_{33}q_{z}^{2}) + [n_{x}(\mathbf{q})n_{y}^{*}(\mathbf{q}) + n_{x}^{*}(\mathbf{q})n_{y}(\mathbf{q})](K_{11} - K_{22})q_{x}q_{y}.$$
(15)

In matrix form

$$2F_d = \{n_x^*, n_y^*\} \begin{cases} A & C \\ C & B \end{cases} \begin{cases} n_x \\ n_y \end{cases}, \tag{16}$$

where

$$A = K_{11}q_x^2 + K_{22}q_y^2 + K_{33}q_z^2,$$
  

$$B = K_{11}q_y^2 + K_{22}q_x^2 + K_{33}q_z^2,$$
  

$$C = (K_{11} - K_{22})q_xq_y.$$

After diagonalization we find two independent modes (the Orsay modes) (Ref. 6) for each wave vector q, i.e.,

$$2F_d = \{n_1^*, n_2^*\} \begin{cases} K_1(\mathbf{q}) & 0 \\ 0 & K_2(\mathbf{q}) \end{cases} \begin{cases} n_1 \\ n_2 \end{cases}, \tag{17}$$

where

$$K_{\alpha} = K_{\alpha\alpha}(q_x^2 + q_y^2) + K_{33}q_z^2$$
.

The transformation which achieves this diagonalization is a uniform rotation which brings q into the  $e_1$ - $\hat{z}$  plane of an  $e_1, e_2, \hat{z}$ , coordinate system whose orientation  $\theta$ , relative to the  $\hat{x}, \hat{y}, \hat{z}$  coordinate system is q dependent. Thus

where  $\theta$  is the angle between  $\mathbf{q}_1 = (q_x, q_y, 0)$  and the x axis. In the quadratic form of Eq. (17) the degrees of freedom are decoupled, permitting one to apply the equipartition theorem. The mean square of the fluctuation amplitudes<sup>2</sup> is

$$\langle |n_{\alpha}(\mathbf{q})|^2 \rangle = kT/K_{\alpha}V$$
, (19)

where V is the integration volume [Eq. (3)].

The contribution of an external magnetic field to the free energy density depends on the orientation of the field with respect to the director according to

$$2F_m = -\gamma_a (\mathbf{n} \cdot \mathbf{H})^2 , \qquad (20)$$

where  $\chi_a$  is the anisotropy of the diamagnetic susceptibility. For a field parallel to  $\bf n$  we get

$$2F_m = -\chi_a H^2 \{n_x^*, n_y^*\} \begin{cases} 1 & 0 \\ 0 & 1 \end{cases} \begin{cases} n_x \\ n_y \end{cases}, \tag{21}$$

which does not change the symmetry of the problem. Thus the angle  $\theta$  in Eq. (18) remains the same and only the eigenvalues are changed equally by  $\chi_a H^2$  (Refs. 2 and 7). Note that this contribution leads to a destabilization of both modes if  $\chi_a$  is negative.

For a field applied perpendicular to n we get

$$2F_{m} = -\chi_{a}H^{2}\lbrace n_{x}^{*}, n_{y}^{*}\rbrace \begin{cases} 1 + \cos 2\phi & \sin 2\phi \\ \sin 2\phi & 1 - \cos 2\phi \end{cases} \begin{cases} n_{x} \\ n_{y} \end{cases},$$
(22)

where  $\phi$  denotes the angle between the magnetic field and  $\mathbf{q}_{\perp}$  which we take parallel to the x axis. This expression together with Eq. (16) can be diagonalized by a rotation through an angle  $\psi$ . However, the rotation now depends on  $F_m$ ,  $F_d$ , and the angle  $\phi$ :

$$\tan 2\psi = \frac{\chi_a H^2 \sin 2\phi}{\chi_a H^2 \cos 2\phi - (K_{11} - K_{22})q_{\perp}^2} . \tag{23}$$

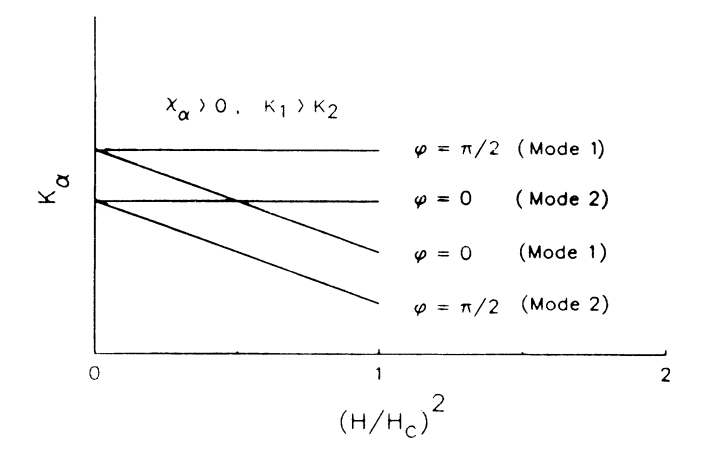


FIG. 2. Dependence of  $K_{\alpha}(q, H)$  on the strength and direction of an applied magnetic field. Assumes  $K_1 > K_2$ .

 $\psi$  is the angle between the  ${\bf e}_1$  directions with and without an applied field. The eigenvalues of the two new modes are

$$F_{\alpha} = \frac{1}{2} (K_{11} + K_{22}) q_{\perp}^{2} + K_{33} q_{z}^{2} - \frac{1}{2} \chi_{a} H^{2}$$

$$\pm \{ \left[ \frac{1}{2} (K_{11} - K_{22}) q_{\perp}^{2} \right]^{2} + \left( \frac{1}{2} \chi_{a} H^{2} \right)^{2} - \frac{1}{2} (K_{11} - K_{22}) q_{\perp}^{2} \chi_{a} H^{2} \cos 2\phi \}^{1/2} , \qquad (24)$$

where +,- corresponds to  $\alpha = 1,2$ , respectively.

In order to see more clearly how the eigenvalues depend on the field consider a field perpendicular to  $\mathbf{q}_{\perp}$  with  $\chi_a > 0$ . In this case we have

$$K_1 = K_{11}q_1^2 + K_{33}q_z^2 (25a)$$

and

$$K_2 = K_{22}q_\perp^2 + K_{33}q_z^2 - \chi_a H^2$$
 (25b)

If the field is parallel to  $\mathbf{q}_1$  we have

$$K_1 = K_{11}q_1^2 + K_{33}q_z^2 - \chi_a H^2$$
, (26a)

$$K_2 = K_{22}q_1^2 + K_{33}q_z^2 \ . \tag{26b}$$

As expected, Eqs. (25) and (26) tell us that the field destabilizes mode 2 (for  $\chi_a > 0$ ) when it lies along the mode-2 axis, i.e., perpendicular to the  $\hat{\mathbf{n}}_0$ -q plane, whereas mode 1 is destabilized when H lies along the mode-1 axis, i.e., in the  $\hat{\mathbf{n}}_0$ -q plane and perpendicular to  $\mathbf{n}_0$  (Fig. 2). Of course, for  $\chi_a < 0$  the field-dependent modes are stabilized rather than destabilized.

# C. Light scattering

Since we restricted our considerations to small fluctuations in a homeotropic sample, the field applied perpendicular to the undistorted director should always be smaller than the critical field for the bend Fréedericksz transition. The lowest-order fluctuation mode wave vector for our sample is near  $\pi/d$  (Fig. 1) due to the strong anchoring obtained by the surface preparation used. Since  $d \sim 55 \ \mu \text{m}$ , observation of this mode requires very small scattering angles in order that the field term be comparable with the elastic terms in the mode-2 geometry selected [see Eq. (25b) and Fig. 3].

To calculate the scattering vector we used

$$q = (k_{xin} - k_{xout}, 0, k_{zin} - k_{zout})$$
, (27)

where the incident wave is extraordinary with8

$$k_{zin} = (n_e/n_0)[(\omega/c)^2 n_e^2 - k_{xin}^2]^{1/2}$$
 (28)

and the scattered wave is ordinary with

$$k_{\text{zout}} = [(\omega/c)^2 n_0^2 - k_{\text{xout}}^2]^{1/2} , \qquad (29)$$

where  $n_e$  and  $n_0$  are the extraordinary and ordinary indices of refraction. Note that according to the refraction law the tangential components of the wave vector are constant on passing an interface between two adjacent media. Therefore, they can be easily determined and adjusted. For an outer medium of refractive index  $n_1$ 

$$k_x = (\omega/c)n_1 \sin\alpha , \qquad (30)$$

where  $\alpha$  is the external angle of incidence or emergence depending on whether  $k_{x \text{in}}$  or  $k_{x \text{out}}$  is calculated.

To account for finite sample size we must modify the limits if integration in the expression for the differential scattering cross section given by<sup>9</sup>

$$\frac{d^{2}\sigma}{d\Omega d\omega} = \pi^{2}\lambda^{-4} \int \int_{-\infty}^{+\infty} \langle \delta \varepsilon^{2} \rangle \times \exp[i(\mathbf{q}^{\text{opt}} \cdot \mathbf{r} - \omega t)] d\mathbf{r} dt ,$$
(31)

where qopt is the optical scattering wave vector, to be dis-

tinguished from the mechanical wave vector  $\mathbf{q}$  appearing in  $n_{\alpha}(\mathbf{q})$ . Specifically for the z direction, after replacing  $\langle \delta \varepsilon^2 \rangle$  by  $\langle |n_{\alpha}(\mathbf{q})|^2 \rangle$  [Eq. (19)], we get

$$\frac{d^2\sigma}{d\Omega d\omega} \propto \int_{-d/2}^{+d/2} \sum_{\alpha,q_z} \langle |n_{\alpha}(q_z)|^2 \rangle \exp[i(q_{\parallel} - q_z)z] dz$$

$$= d \sum_{\alpha,q_z} \langle |n_{\alpha}(q_z)|^2 \rangle \frac{\sin(q_{\parallel} - q_z)d/2}{(q_{\parallel} - q_z)d/2} , \quad (32)$$

where the  $q_z$  are the  $q_z(n)$  defined by Eqs. (11) and (12) and  $q_{\parallel}$  is the geometrically adjustable z component of the scattering vector  $\mathbf{q}^{\mathrm{opt}}$ . We see that the finite sample size leads to an uncertainty in the selection of  $q_z$  [single slit interference function in Eq. (32)]. This allows several modes to contribute to light scattering in a given direction. However, the predominant modes are those within the interval

$$q_{\parallel} - 2\pi/d < q_{z}(n) < q_{\parallel} + 2\pi/d$$
 (33)

This yields a smoothing of the angular distribution of scattered light which is sufficient to explain why there are no fringes despite the expected discrete mode spectrum. It also permits one to adjust  $q_{\parallel} < q_z(0) \le \pi/d$  and thus study the behavior of the lowest-order fluctuation mode without the necessity for an exact coincidence of  $q_{\parallel}$  and  $q_z(0) = q_0$  (see Table I).

In addition to the slit function in Eq. (32) one must account for the geometric factor<sup>6</sup> left out of Eqs. (31) and (32) which selects mode 1 and/or mode 2 and which leads to a further modification of the intensities. Because of this and the difficulty of accounting for stray light the determination of relaxation times by photon autocorrelation is used instead of intensity measurements.

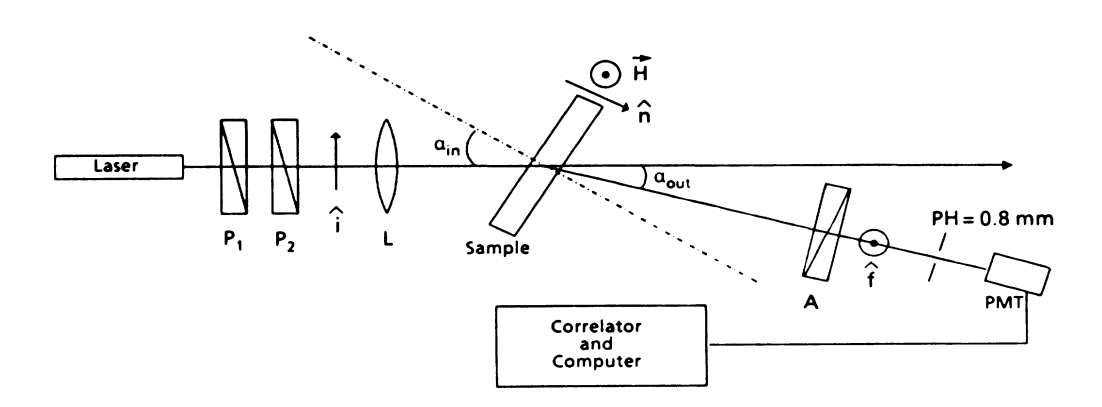


FIG. 3. Experimental setup and scattering geometry.  $P_1$ , polarizer for intensity scaling;  $P_2$ , polarizer, vertical; A, analyzer, horizontal; PMT, photomultiplier tube; PH, pin hole 0.8 mm diameter; L, focusing lens; H, magnetic field;  $\hat{i}$ ,  $\hat{f}$ , the incoming and outgoing polarization states;  $\hat{n}$ , the direction of the liquid-crystal director; sample, homeotropically aligned DHAOB; and  $\alpha_{\text{in,out}}$ , angles of incidence and emergence, respectively (note: these are external angles).

Case	$(10^9  \mathrm{m}^{-2})$	$(10^9 \frac{q_{\parallel}^2}{\mathrm{m}^{-2}})$	$q_0^2 = (\pi/d)^2$ (10° m <sup>-2</sup> )	$lpha_{ m in}$	$lpha_{ m out}$	
1	0.00	1.26	3.26	12.86°	12.86°	
2	0.67	0.93	3.26	12.86°	12.77°	
3	6.30	0.0004	3.26	1.43°	0.97°	
4	11.20	0.0009	3.26	1.43°	0.82°	

TABLE I. Scattering geometry used for all four cases.

### D. Director dynamics

Neglecting inertial effects the time dependence of the fluctuation modes can be described<sup>2</sup> by

$$\frac{\partial}{\partial t} n_{\alpha}(q) = -\frac{1}{\tau_{\alpha}(q)} n_{\alpha}(q) , \qquad (34)$$

which gives rise to a single exponential correlation function with an inverse correlation time given by

$$\tau_{\alpha}^{-1}(q) = K_{\alpha}(q) / \eta_{\alpha}(q)$$
 (35)

 $K_{\alpha}(q)$  is in general given by Eq. (24). The effective viscosity  $\eta_{\alpha}(q)$  was first derived in Ref. 6 with the assumption of an infinitely extended sample volume. Pieransky, Brochard, and Guyon<sup>4</sup> showed that the presence of confining walls leads to a hindrance of backflow which increases the effective viscosity. A detailed treatment of this question will be the subject of a separate paper. Here we consider the viscosity as an adjustable parameter which is to be determined experimentally.

### III. EXPERIMENT, RESULTS, AND DISCUSSION

The experimental setup used here is shown in Fig. 3. A 55  $\mu$ m homeotropic sample of dihexylazoxybenzene (DHAOB) was placed between the pole faces of a magnet. Homeotropic alignment was achieved on glass slides coated with an organosilane surfactant. 10 Vertically polarized light incident at an angle  $\alpha_{in}$  excited an extraordinary incident wave in the liquid crystal, which was filtered (0.2  $\mu$ m) to remove particulate matter. The scattered light leaving the sample at angle  $\alpha_{out}$  was observed through a horizontal polarizer. Since the director was in the scattering plane and the magnetic field was applied perpendicular to it we expect to observe the destabilization of mode 2 according to Eq. (25b). In order to vary the scattering vector the four sets of incidence and emergence angles given in Table I were used. These will be referred to as cases one through four.

In all the experiments the correlation function could be fitted with reasonable accuracy to a single exponential function [as Eq. (34) predicts] plus a baseline. For the extreme heterodyne case<sup>11</sup> one has

$$g(t) = A[1 + B \exp(-t/\tau)],$$
 (36)

and for the homodyne case,

$$g(t) = C[1 + D \exp(-2t/\tau)].$$
 (37)

The ratio  $g(0)/g(\infty)$  was used to distinguish between

homodyne and heterodyne regimes. Despite the use of crossed polarizers, for cases one and two (Table I), involving nearly forward scattering, the contribution of the main beam was large enough to cause heterodyning with B typically  $10^{-3}$ . In cases three and four (Table I) we obtained  $D \ge 0.7$  indicating homodyning. In the case of homodyning the coefficient D is F(A), a geometric factor which can be made nearly unity by exposing an area on the photocathode no larger than a coherence area. A pin hole of the appropriate size was used to ensure that F(A) was of the order of 1. The homodyne data verified this.

Case one, pure forward scattering  $(\alpha_{\rm in} = \alpha_{\rm out})$ , probes  $q_x = 0$  according to Eq. (30). Note that the optical and mechanical wave vector components perpendicular to  $\bf n$  are equal due to the continuous nature of  $q_x$ , therefore we do not distinguish between  $\bf q_x$  and  $q_x^{\rm opt}$  below. In contrast to Ref. 3 the sample was inclined with respect to the main beam, leading to  $q_{\parallel} \neq 0$ ; however  $q_{\parallel}$  is smaller than the expected lowest mode  $q_z = \pi/d$ . The scattered intensity is not zero as it would be for normal incidence. The scattering vector in case two was chosen such that  $q_x \sim q_{\parallel}$ , both being smaller than  $\pi/d$ . Cases three and four were chosen to give values of  $q_x$  that are larger than  $\pi/d$  but small enough to observe the contribution of the destabilizing field.

It can be seen from Fig. 4 that the dependence of the inverse correlation times on the square of the magnetic field strength is in good agreement with Eqs. (25b) and (35). The appropriate equation to fit the data in Fig. 4 is

$$\tau^{-1} = A - BH^2 , \qquad (38a)$$

where

$$A = (K_{22}q_x^2 + K_{33}q_0^2)/\eta , (38b)$$

$$B = \chi_a / \eta \tag{38c}$$

and  $\tau$  is the relaxation time obtained from the correlation function.  $K_{22}$  and  $K_{33}$  are the twist and bend elastic coefficients and  $q_0 = \pi/d$ . The measured slope and  $\chi_a$  (Ref. 13) were used to calculate the effective viscosity  $\eta$  (Table II).

It is interesting to note the equivalence of  $\tau_{1,2}^{-1}$  versus  $H^2$  for cases 1 and 2 although the optical wave vectors were quite different. This result is naturally explained by the theoretical analysis presented here. In the strong anchoring limit  $[q_z(0)=q_0=\pi/d]$  both of these experiments are off mode, i.e.,  $\mathbf{q}^{\text{opt}}$  is not coincident with  $\mathbf{q}=(q_x,q_z(n))$ . Therefore, one could only have scattered

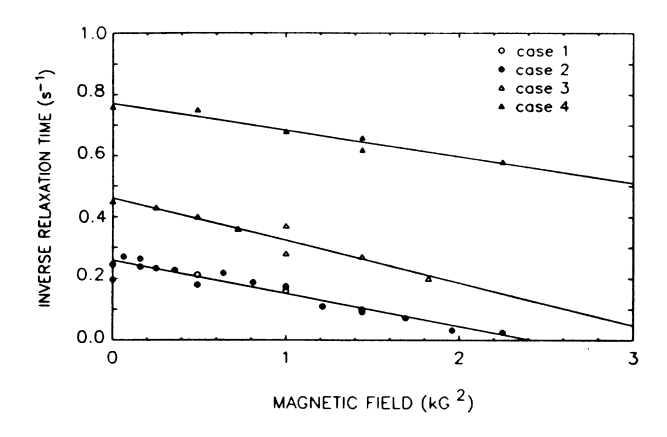


FIG. 4. Graph of inverse relaxation time vs the square of the magnetic field.

light due to interference effects [Eq. (32)]. The fact that  $\tau_1(H) \sim \tau_2(H)$  strongly suggests that this scenario is true and, further, that the mode observed in case 1 is the lowest-order mode  $(q_x=0,q_z(n)=q_z(0))$  with  $q_z(0) \sim q_0=\pi/d$ , while the mode observed in case two is  $(q_x\neq 0,q_z(n)=q_z(0))$ . Case 2 has nearly the same relaxation rate as case 1 because  $q_x^2 \ll q_0^2$  and, typically,  $K_{22} < K_{33}$  (see also below). To complete the scenario it must be noted that both energetics and the interference function strongly suppress scattering from modes with  $q_z \geq q_z(1)$  by comparison with the modes discussed.

A separate measurement of the bend Fréedericksz transition gave  $H_{c3}^2 = 2.40 \, (\text{kG})^2$  (Ref. 14) in good agreement with the values obtained from the intercepts of  $\tau^{-1}$  vs  $H^2$  for cases 1 and 2 (Table II). (Using the published value of  $\chi_a$  (Ref. 13),  $d=55 \, \mu\text{m}$  and  $H_{c3}^2 = 2.40 \, (\text{kG})^2$  in the usual Fréedericksz transition equation gives  $K_{33} = 8.8 \times 10^{-7} \, \text{dyn.}$ ) Thus, the interpretation that cases 1 and 2 are dominated by scattering from normal modes of wave vector  $(q_x, q_0 \sim \pi/d)$ , is consistent with all aspects of our results.

Finally we note that the ratio  $K_{22}/K_{33}$  at  $\sim 22$  °C may be determined by comparison of cases 1 and 4. Specifically one has

$$\frac{\tau_4^{-1}(0)}{\tau_1^{-1}(0)} = \frac{A_4}{A_1} = \frac{\eta_1 (K_{22}^2 q_x + K_{33}^2 q_0)_4}{\eta_4 (K_{33} q_0^2)_1} , \tag{39}$$

which leads to

$$\frac{K_{22}}{K_{33}} = \left[ \frac{\eta_4 A_4}{\eta_1 A_1} - 1 \right] \frac{q_0^2}{q_x^2} \sim 0.7 , \qquad (40)$$

where  $A_4$  and  $A_1$  are the  $H^2=0$  intercepts of Fig. 4,  $\eta_4$  and  $\eta_1$  are given in Table II, and  $q_0^2=(\pi/d)^2$  and  $q_x^2$  are given in Table I. A check of this result can be made by noting that  $\tau_1^{-1}(H_c)=\tau_4^{-1}(H_c)=0$  leads to

TABLE II. Measured critical fields and viscosities for each

Case	T (°C)	$H_c^2$ (kG <sup>2</sup> )	η (cP)
1	22	2.52	108±(13)
2	22	2.30	90±(5)
3	20.5	4.39	77±(9)
4	21.5	8.88	125±(19)

$$\frac{H_c^2(4)}{H_c^2(1)} = \frac{(K_{22}q_x^2 + K_{33}q_0^2)_4}{(K_{33}q_0^2)_1}$$
(41)

or

$$\frac{K_{22}}{K_{33}} = \frac{q_0^2}{q_x^2} \left[ \frac{H_c^2(4)}{H_c^2(1)} - 1 \right] \sim 0.7 , \qquad (42)$$

in agreement with the above result. Thus we have confirmed our assumption above that  $K_{22}/K_{33} < 1$  and further substantiated the central conclusion that cases 1 and 2 are dominated by scattering from lowest-order normal mode with  $q_z = q_z(0) = q_0$  (strong anchoring).

## IV. CONCLUSION

In the discussions above we have shown theoretically that for the case of finite anchoring the lowest-order fluctuation modes have a nonzero Fourier component  $q_z \leq \pi/d$ . Such modes were observed experimentally in cases one and two where the optical wave vector component  $q_{\parallel}$  was smaller than  $\pi/d$ . The experimental results for cases one and two are expected if the sample has lowest-order modes with a z component of wave vector near  $\pi/d$  (strong anchoring). In addition, the inverse relaxation time decreases linearly with the square of the magnetic field as predicted.

Finally we note that the class of experiments performed are capable of high accuracy determinations of Fréedericksz fields without the need for finite static distortion. The scatter in the data in Fig. 4 are primarily due to the fact that the sample temperature was not controlled and the material studied exhibits a nematic-smectic A transition (where  $K_{33}$  diverges) only a few degrees below the temperatures of the experiments. The temperatures (Table II) represent averages of fluctuating room temperature measurements made during each experiment.

# **ACKNOWLEDGMENTS**

We acknowledge National Science Foundation Solid State Chemistry Program support under Grants Nos. DMR 87-03524 and DMR 88-18561.

- \*Permanent address: Sektion Physik der Karl-Marx-Universität Leipzig, Linnéstrasse 5, Leipzig, DDR-7010, German Democratic Republic.
- <sup>1</sup>V. Fréedericksz and V. Zwetkoff, Phy. Z. Sowjetunion **6**, 490 (1934).
- <sup>2</sup>P. G. de Gennes, *The Physics of Liquid Crystals* (Clarendon, Oxford, 1974).
- <sup>3</sup>S. M. Arakelyan, L. E. Arushanian, and Yu. S. Chiligaryan, Zh. Tekh. Fiz. **56**, 1949 (1986) [Sov. Phys. Tech. Phys. **31**, 1165 (1986)].
- <sup>4</sup>P. Pieranski, F. Brochard, and E. Guyon, J. Phys. (Paris) 34, 35 (1973); see M. Sefton, A. Bowdler, and H. Coles, Mol. Cryst. Liq. Cryst. 129, 1 (1985) for an interesting study of the film thickness dependence of mode-2 relaxation rates in homeotropic geometry.
- <sup>5</sup>A. Rapini and M. Papoular, J. Phys. (Paris) Colloq. **30**, C4-54 (1971).
- <sup>6</sup>Orsay Group, J. Chem. Phys. **51**, 816 (1969).
- <sup>7</sup>M. Malraison, Y. Poggi, and E. Guyon, Phys. Rev. A **21**, 1012 (1980).
- <sup>8</sup>K. Eidner, G. Mayer, M. Schmidt, and H. Schmiedel (unpublished).
- <sup>9</sup>S. Chandrasekhar, *Liquid Crystals* (Cambridge University Press, Cambridge, England, 1980).
- <sup>10</sup>Removing  $W_0$  from the integral in Eq. (2) assumes that it has a well-defined average value over length scales appropriate to the continuum approximation [see, for example, M. Warner,
- Mol. Phys. 52, 677 (1984)] and that this average is constant over the integration surface. In our light-scattering experiment this would be the part of the surface illuminated by the laser beam. Allowing  $W_0$  to be some random function of position in Eq. (2) would invalidate the assumed mode structure [Eq. (6)] and may make the problem analytically intractable, though highly interesting from both basic and practical perspectives. Our surface preparation was carried out on a clean (filtered air flow) table using filtered (0.2-\mu m) surfactant solution. Nevertheless, we cannot make precise statements about the uniformity of  $W_0$ . Such statements would require surface analyses beyond the scope of this work. However, uniformity of director orientation was tested down to length scales of  $\sim 1$ μm by polarizing microscope observations, which revealed no detectable director distortions in the central 5-mm-diam region of the film within which the laser beam was focused. An even more stringent test of director uniformity is the extinction ratio e with the sample between high-quality polarizers. e was the same  $(1.3 \times 10^5)$  within experimental uncertainty  $(\pm 20\%)$  with and without the sample present.
- <sup>11</sup>R. Pecora, *Dynamic Light Scattering* (Wiley, New York, 1976), see Chap. 4.
- <sup>12</sup>H. Z. Cummins and E. R. Pike, Photon Correlation and Light Beating Spectroscopy (Plenum, New York, 1974).
- <sup>13</sup>M. Achard, F. Hardouin, G. Sigaud, and H. Gasparoux, J. Chem. Phys. **65**, 1387 (1976).
- <sup>14</sup>H. K. M. Vithana and D. L. Johnson (unpublished).